Extragalactic jets. I - Trajectories. II - Shape and stability

Smith, M.D.; Norman, C.A.

Extragalactic jets − I. Trajectories

M. D. Smith *Department of Theoretical Physics, 1 Keble Road, Oxford OX1 3NP and Department of Physics, University of Illinois at Urbana-Champaign, Urbana, Illinois 61801, USA*

C. A. Norman *Huygens Laboratorium, University of Leiden, Wassenaarseweg 78, 2300 RA Leiden, The Netherlands*

Summary. A detailed analytical model is presented for the propagation of jets through various inhomogeneous media typical of extragalactic radio source environments. Observing that all jets have small opening angles, the determination of their path and shape becomes analytically tractable. The structure of jets is calculated under the assumptions that there is a steady irrotational flow which is both compressible and isentropic; that the jet is confined, so that a pressure equilibrium is maintained; and that viscous forces are negligible across the jet−intergalactic medium interface.

We find that significant jet-bending can only occur if the characteristic Mach number is less than unity and the jet is initially directed at a large angle to the direction of the external pressure gradient. The higher the Mach number, the less the jet-bending. Ultra-relativistic jets will only bend through $\sim 1/\Gamma$ radians, where Γ is the jet Lorentz factor. Our calculations of jet-paths under various conditions can adequately account for much of the observed morphology of bending of extragalactic radio source jets, and are consistent with statistical studies of the correlation of radio with optical morphology.

1 Introduction

Detailed maps of radio sources with jets clearly show that jets bend (Miley 1980). The bending occurs over a range from ~ 1 pc to ~ 1 Mpc (Van Breugel & Miley 1977; Readhead *et al.* 1978; Bridle *et al.* 1979). It seems plausible that the bending is caused by pressure gradients in the jet's environment influencing the jet's trajectory.

An extreme example of such a phenomenon has already been discussed using a simple model for the head−tail source NGC 1265 (Begelman, Rees & Blandford 1979; Jones & Owen 1979). We develop here a more sophisticated analytical model which can be used to study the jet-bending phenomenon itself.

Our model is based on the one-dimensional jet model of Blandford & Rees (1974), extended to three dimensions under our assumption that the jet is thin, and relaxing their

assumptions of a straight jet-path and a circular cross-sectional shape. Moreover, from the observed path and shape of a jet, we infer properties of the interstellar medium around it.

Section 2 discusses the basic model and its assumptions in general terms. In Section 3, the formulae and method for analysing non-relativistic jets are set out. We obtain the trajectory of a jet in terms of its initial conditions and the nature of the surrounding medium. Section 4 demonstrates how these results extend to ultra-relativistic jets. The physical and observational implications of our model are discussed in Sections 5 and 6, respectively.

2 The bent-jet model

We assume that a jet is a low-density, isentropic fluid with a weak magnetic field. The model will be applied to both relativistic and non-relativistic jets; and in each case, the jet will be assumed to be initially confined.

The density of the jet fluid is required to be much less than the density of the surrounding medium in the galactic nucleus or wherever the jet is formed. Thus, buoyancy forces will dominate gravitational forces and the jet fluid will be accelerated out of the source region. Outside this core region, the confined jet model may become inappropriate, as seems to be the case for both 3C 449 and 3C 31, whose jets have particle densities estimated to be 10^{-2} cm^{-3} and probably expand freely (Perley, Willis & Scott 1979).

We argue that a thin region or boundary layer of turbulent (non-isentropic) flow separates the irrotational jet flow from the external medium. The drag force at this boundary layer will be assumed to have a negligible effect on the jet flow; and the boundary layer will simply be represented by a velocity discontinuity. This boundary condition is observationally supported by the absence of limb brightening in resolved jets (A. G. Willis 1980, private communication), suggesting that we are seeing radiation from the jet itself, rather than a surrounding sheath. The jet fluid is taken to be inviscid; and the entrainment of matter through the Kelvin–Helmholtz instability is ignored. In general, we propose that the boundary layer dissipation is sufficiently low for the flow to be taken as isentropic.

The pressure external to the jet, p_e, is taken to be a given function of position alone, and axisymmetric around one axis of a Cartesian coordinate system (X, Y, Z) whose origin coincides with the origin of the jet. Such a distribution can be described by

$$p_e = p_0 \cdot \{\exp(-k_1^2 X^2 - k_1^2 Y^2 - k^2 Z^2)\}, \tag{1}$$

or

$$p_e = \frac{p_0}{3} \left\{ \left(\frac{X}{h_1}\right)^m + \left(\frac{Y}{h_1}\right)^m + \left(\frac{Z}{h}\right)^n \right\}, \tag{2}$$

where k, k_1, h, h_1 are constant characteristic scales and p_0 is constant. If $h_1 \gg h$ and $k_1 \ll k$, equations (1) and (2) can be written,

$$p_e = p_0 \exp(1 - k^2 Z^2), \tag{3}$$

$$p_e = p_0 \left(\frac{Z}{h}\right)^n, \tag{4}$$

so that Z represents the distance from the 'central plane' of a highly flattened gas cloud. Equation (3) thus describes an isothermal gas cloud within, and gravitationally supported by, a uniform ellipsoidal mass distribution, while the variable index n in equation (4) allows an approximation to either isothermal or adiabatic atmospheres. The one-dimensional pressure

variations are not restrictive; for, through rotation of axes, we can obtained pressure distributions of the form $p_e \propto Z^n + NY^n$, where N is a constant.

The jet flow is fully determined on application of the following initial conditions. These are assumed to be given on the boundaries $Z = 1/k$ (equation 3) and $Z = h$ (equation 4) by the pressure $p = p_0$, density $\rho = \rho_0$, cross-sectional area $A = A_0$, cross-sectional shape $\tilde{S}_0$, and fluid velocity $\mathbf{v}_0$ at an angle Ω_0 to the major plane. The presumption is thus made that a steady jet is established and maintained by processes within the core.

An important inference from the observations is that jets are thin in comparison with their length. A measure of the slenderness of a beam is defined by Keller & Weitz (1952) as

$$\epsilon = \text{slenderness ratio} \equiv \frac{\text{typical beam half-width}}{\text{typical beam length}}.$$

Typical numerical values for the slenderness ratio of jets are $\epsilon \sim 0.1$ for 3C 449, $\epsilon \sim 0.05$ for NGC 6251, and $\epsilon \sim 0.2$ for NGC 315. For jets in more powerful extended sources, a maximum value of the ratio can be inferred from the sizes of the hot spots which form at the interface of a jet with the intergalactic medium. The hot spots are typically 3 kpc wide at distances of the order of 150 kpc, giving $\epsilon \leqslant 0.01$.

3 Non-relativistic jets

Previous studies of thin jets have dealt with incompressible fluids acting under a constant gravitational force, and comparisons have been made with jets of water (Keller & Weitz 1957; Keller & Geer 1973; Tuck 1976). A detailed three-dimensional analysis of such flows has been given by Geer (1977a, b) whose basic method is extended here to compressible fluids and boundary conditions relevant to extragalactic jets. The calculation to zeroth order in the slenderness ratio gives the jet's trajectory. The variations in the magnitude of the parallel velocity component calls for motion across the flow in order to conserve mass. These cross-flow velocities determine the shape of the jet, which is obtained with higher order calculations.

The model jet consists of an isentropic fluid that is inviscid and compressible and is in steady and irrotational motion. By using the same Bernouilli constant across the jet and assuming irrotational flow the model is reduced to a simple set of equations. An adiabatic equation of state with index γ is used:

$$\frac{p}{p_0} = \left(\frac{\rho}{\rho_0}\right)^\gamma. \tag{5}$$

Energy and mass conservation lead to a Bernouilli equation satisfied throughout the jet, with velocity potential Φ:

$$(\nabla\Phi)^2 + \frac{2\gamma}{\gamma-1}\frac{p}{\rho} = U^2, \tag{6}$$

where

$$U^2 = v_0^2 + \frac{2\gamma}{\gamma-1}\left(\frac{p_0}{\rho_0}\right)$$

is a constant, and

$$\nabla \cdot (\rho\nabla\Phi) = 0. \tag{7}$$

Equation (7) can then be written as a Poisson equation:

$$(\gamma - 1)\{U^2 - (\nabla\Phi)^2\} \nabla^2\Phi = (\nabla\Phi \cdot \nabla)(\nabla\Phi)^2. \tag{8}$$

This is the general potential equation for (non-relativistic) steady compressible fluid flow. In the incompressible case ($\gamma \to \infty$), this reduces to Laplace's equation, $\nabla^2\Phi = 0$.

A boundary condition is specified through the velocity normal to the surface being zero,

$$\mathbf{n} \cdot \nabla\Phi = 0, \tag{9}$$

where $\mathbf{n}$ is the unit outward normal to the surface. Using equations (5) and (6), the pressure equilibrium across the bounding surface can be written as

$$(\nabla\Phi)^2 = U^2 - \frac{2\gamma}{\gamma - 1} \frac{p_0^{1/\gamma}}{\rho_0} p_e^{1-1/\gamma}. \tag{10}$$

The remaining problem is to find a solution to equation (8) satisfied throughout the jet, with equations (9) and (10) satisfied on the jet surface. Since the external pressure is axisymmetric, there is some freedom in fixing the plane in which the initial jet velocity, $\mathbf{v}_0$, is directed. Here it is taken to be on the $Y-Z$ plane. Although it is not necessary to specify the nature of the flow further, from the X-independence of the pressure distributions it is obvious that the locus, C, of centroids of mass of the jet remains in the $Y-Z$ plane. Allowing for torsion only complicates the analysis and, of course, the torsion is eventually found to be zero for the curve C!

We can now proceed to derive the solution to the jet-path to zeroth order in the slenderness parameter. The mathematical details can be found in Smith (1979).

3.1 COORDINATE SYSTEM

We choose a coordinate system as indicated in Fig. 1. The origin of the system lies on the centroids of mass and so the directions of the orthogonal axes are not fixed. K is the curvature of C [where C is given by $Y(\sigma), Z(\sigma)$] defined as

$$K^2 = \left(\frac{\partial^2 Y(\sigma)}{\partial \sigma^2}\right)^2 + \left(\frac{\partial^2 Z(\sigma)}{\partial \sigma^2}\right)^2. \tag{11}$$
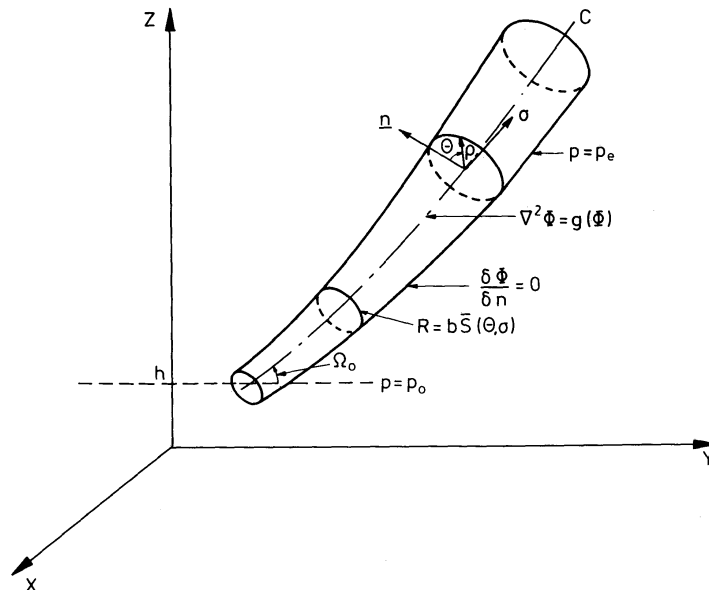

Figure 1. A sketch of a thin jet indicating the type of flow discussed and the coordinate system.

The boundary surface of the jet will be described by $R = b_0 \widetilde{S}(\theta, \sigma)$, where b_0, given by $A_0 = \pi b_0^2$, measures the typical initial jet half-width, and $\widetilde{S}$ determines the cross-sectional shape.

Re-defining the coordinates by $r = R/b_0$, $s = \sigma/h$ and $(x, y, z) = (X, Y, Z)/h$, equation (4) is reduced to $p_e = p_0 z^n$. Accordingly, we define,

$$\epsilon = b_0/h, \quad S(\theta, s; \epsilon) = \widetilde{S}(\theta, \sigma), \quad \Phi(r, \theta, s; \epsilon) = \frac{\Phi(R, \theta, \sigma)}{Uh} \quad \text{and} \quad \xi = \frac{2\gamma}{\gamma - 1} \frac{p_0}{\rho_0 U^2}, \tag{12}$$

where ξ is related to the initial Mach number, M_0, of the flow by

$$M_0^2 = \frac{2}{\gamma - 1}(1/\xi - 1), \tag{13}$$

as demonstrated in Fig. 2. Here, $n\xi$ is the ratio of the initial mean radius to the external pressure scale-height, and ξ is a measure of the relative importance of the initial pressure and the initial momentum flux density.
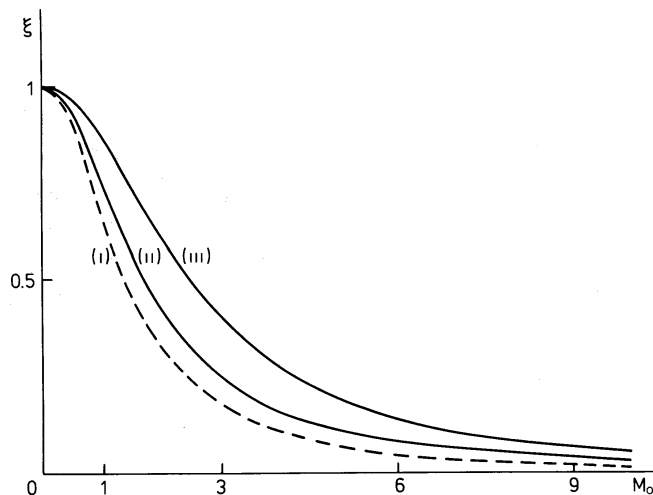

Figure 2. The relation between the parameter ξ used in the text and the initial Mach number. Curve (i) holds for ultra-relativistic fluids. Non-relativistic fluids with (ii) $\gamma = 5/3$ and (iii) $\gamma = 4/3$ are also shown.

3.2 ASYMPTOTIC EXPANSION

The assumption is now made that as ϵ tends to zero, ϕ and s have power series expansions in ϵ of the form,

$$\phi(r, \theta, s; \epsilon) \sim \sum_{j=0}^{\infty} \phi^j(r, \theta, s)\epsilon^j, \tag{14}$$

$$S(\theta, s; \epsilon) \sim \sum_{j=0}^{\infty} S^j(\theta, s)\, \epsilon^j, \tag{15}$$

where the ϕ^j and S^j are independent of ϵ.

The functions ϕ^j and S^j are determined by substituting these expansions into our set of equations and making Taylor expansions in ϵ about $\epsilon = 0$.

3.3 ZERO-ORDER SOLUTION

Using the identity $\dot{y}^2 + \dot{z}^2 = 1$, and the initial conditions (Section 2), the locus of centroids of mass of the jet can be calculated

$$\frac{1 + (dz/dy)^2}{1 + \tan^2 \Omega_0} = \frac{1 - \xi z^\mu}{1 - \xi}, \tag{16}$$

where $\mu = n(1 - 1/\gamma)$, which can be written in the form

$$\frac{\cos \Omega}{\cos \Omega_0} = \left(\frac{1 - \xi}{1 - \xi z^\mu} \right)^{1/2}, \tag{17}$$

where $\Omega = \tan^{-1}(dz/dy)$. The solution to this equation is,

$$y - 1 = \mu^{-1} \xi^{1/\mu} \left(\frac{1 - \xi}{m_0^2 + \xi} \right)^{1/2} \left(\frac{m_0^2 + \xi}{m_0^2 + 1} \right)^{1/\mu} \int_\alpha^{\alpha z^\mu} (1 - \omega)^{-1/2} \omega^{(1-\mu)/\mu} \, d\omega, \tag{18}$$

where

$$\alpha = \xi \frac{m_0^2 + 1}{m_0^2 + \xi} \quad \text{and} \quad m_0 = \tan \Omega_0.$$

The right-hand side of equation (18) is a multiple of the open beta function, $\beta_0(1/\mu, 1/2)$ (Abramowitz & Stegun 1965). (The solution in the case of a homogeneous external pressure is given by $n = 0$. Since $\mu = n(1 - 1/\gamma)$, a straight jet with $dz/dy = m_0$ results, as expected.)

The analysis of the previous two subsections can easily be generalized to any atmosphere of the form $p_e = p_0 f(z)$; $f(z)$ is an analytical function, suitably scaled so that $p_e = p_0$ at $z = 1$. Then in the case of $\kappa \neq 0$, on application of the initial conditions, two non-linear differential equations for the locus of centroids of mass of the jet are obtained:

$$2(\ddot{y}^2 + \ddot{z}^2) + \frac{\xi \nu \ddot{z} f^{\nu-1}(z)}{1 - \xi f^\nu(z)} \frac{df}{dz} = 0, \tag{19}$$

$$\dot{y}^2 + \dot{z}^2 = 1, \tag{20}$$

where $\nu = 1 - 1/\gamma$. These may be integrated to give the jet-path in the form,

$$\frac{1 + (dz/dy)^2}{1 + m_0^2} = \frac{1 - \xi f^\nu(z)}{1 - \xi}. \tag{21}$$

4 Relativistic jets

In this section, the three-dimensional relativistic equations of motion for a flow within a thin jet are discussed. For simplicity, the case of an isotropic ultra-relativistic fluid is taken and the flow characteristics as determined in Section 2 are applied. The enthalpy per unit proper volume can thus be written as

$$\omega = 4p \propto \rho^{4/3}, \tag{22}$$

where p is the pressure measured in the comoving frame and ρ is the proper mass density. This can be written as an adiabatic gas law:

$$\frac{p}{p_0} = \left(\frac{\rho}{\rho_0} \right)^{4/3}. \tag{23}$$

The relativistic Bernoulli equation is given by $\omega\Gamma/\rho$ being a constant along any stream-line (Landau & Lifshitz 1959). Here, Γ is the Lorentz factor $(1 - v^2/c^2)^{-1/2}$, where v is the fluid velocity. Here, γ denotes the adiabatic index; hence Γ is used for the Lorentz factor. Using equations (22) and (23), this becomes,

$$\frac{p}{P_0} = \left(\frac{\Gamma_0}{\Gamma}\right)^4, \tag{24}$$

where

$$\Gamma_0 = \left(1 - \frac{v_0^2}{c^2}\right)^{-1/2}.$$

The relativistic equation for potential flow is

$$\nabla \times \left(\frac{\omega}{n}\mathbf{u}\right) = 0$$

where $\mathbf{u}$ gives the spatial components of the velocity four-vector, i.e. $\mathbf{u} = \Gamma\mathbf{v}$. The potential function, Φ, is written here as

$$\left(\frac{p}{p_0}\right)^{1/4}\mathbf{u} = \nabla\Phi, \tag{25}$$

upon using equations (22) and (23). Steady potential flow requires equation (24) to be satisfied everywhere in the fluid. The conservation of the number of fluid particles is given by $\nabla \cdot (\rho\mathbf{u}) = 0$. Using equation (23), we obtain

$$\nabla \cdot (p^{3/4}\mathbf{u}) = 0. \tag{26}$$

Four equations for the four unknowns, p, ρ, v and Φ, have been found. Combining equations (24), (25) and (26) yields $\Gamma_0 v = \nabla\Phi$ and

$$\{c^2\Gamma_0^2 - (\nabla\Phi)^2\}\nabla^2\Phi = (\nabla\Phi \cdot \nabla)(\nabla\Phi)^2, \tag{27}$$

satisfied everywhere in the fluid. Identifying $\Gamma_0 c \equiv U$, we then have the equivalent of the non-relativistic fluid equation (8) with an adiabatic index, γ, of 2.

As with the non-relativistic jet, the boundary condition $\mathbf{n} \cdot \nabla\Phi = 0$ is incorporated using the requirement that the velocity normal to the surface is zero. Consequently, the pressure exerted transverse to the boundary surface is identical to the pressure in the comoving frame. From equation (24), the pressure balance across the boundary gives

$$(\nabla\Phi)^2 = U^2 - c^2\left(\frac{p_e}{p_0}\right)^{1/2}. \tag{28}$$

By rescaling physical quantities as in equation (12), except for ξ which is now given by $\xi = 1/\Gamma_0^2$, the equations are reduced to the form given in Section 3, with $\gamma = 2$. Hence the previous results for ϕ and the jet-path hold. By defining an initial Mach number as

$$M_0 = \sqrt{(2/3)}\frac{\Gamma_0 v_0}{c_s},$$

where $c_s = c/\sqrt{3}$ is the sound-speed in an ultra-relativistic plasma, the relationship

$$M_0^2 = 2(1/\xi - 1) \tag{29}$$

is obtained, as shown in Fig. 2.

We now discuss some physical and observational implications of the bent-jet model calculated in the preceding sections.

5 Physical implications

5.1 FLOW VELOCITY

The Mach number M, defined as v/c_s in the non-relativistic case and as $\sqrt{(2/3)}\Gamma v/c_s$ in the relativistic case, is given in terms of non-dimensional parameters by

$$M^2 = \frac{2}{\gamma - 1} \frac{1 - \xi z^\mu}{\xi z^\mu}, \tag{30}$$

for power law external atmospheres with $\mu = n(1 - 1/\gamma)$. The external pressure is taken to be a monotonically decreasing function of z, $(n < 0)$, and the adiabatic index, γ, is taken to be greater than unity, so that $\mu < 0$. For example, a jet propagating through a radio lobe may be confined by a surrounding 'cavity' of plasma that results from the earlier ejection of energy from the core (Scheuer 1974) and, in this case, $n \sim 0$. Therefore, the Mach number increases monotonically with distance from the core. For $z \gg 1$ or $M_0 \gg 1$ (i.e., $\xi \ll 1$), the increase, $M \propto z^{-\mu/2}$, is slow.

As shown by Blandford & Rees (1974), an initially subsonic flow at the centre of a galactic nucleus will become supersonic within a short distance, when the pressure has decreased by a factor $[2/(\gamma + 1)]^{\gamma/(\gamma - 1)} \sim \frac{1}{2}$ from its value where the fluid velocity is zero (stagnation point). For the non-relativistic model to be applicable, it must be verified that the jet velocity remains non-relativistic all along the flow. If the stagnation sound-speed is relativistic, however, the fluid velocity then also becomes relativistic within a pressure scale-height. So a non-relativistic stagnation sound-speed, c_s, is required. Then, as $z \to \infty$, $v^2 \to U^2 = 2/(\gamma - 1)c_s^2$. It is here proposed that a cloud of non-relativistic gas accumulates at the centre of the nuclear core of a galaxy. The cloud must be a great deal larger than the Schwartzschild radius of any mass concentration within it; since, near this radius, the sound-speed of a pressure-supported gas is relativistic. When the central pressure is raised, a high pressure gradient is attained and the light gas flows out of the core.

5.2 JET-PATH

The jet-path is independent of the cross-sectional shape. In Fig. 3(a) and (b), the path of a jet (the locus of centroids of mass) is shown. By using equation (21), the equation of motion for the jet-path can be derived

$$\rho v^2 K = (-dP/dZ) \cos \Omega, \tag{31}$$

indicating that the centrifugal force is balanced with the force due to the pressure gradient across the jet. The curvature is a monotonically decreasing function of z, i.e., the bending is predominantly occurring close to the origin of the jet. If the external pressure decreases slowly with increasing z, then the bending is more gradual (Fig. 3a). With the exponential atmosphere given by equation (3), 80 per cent of the jet-bending occurs within one scale-height.

The dependence of the jet-path on the initial injection angle Ω_0 and Mach number M_0 is demonstrated in Fig. 3(b). The total bending of a jet, $\Omega_F - \Omega_0$, is a function of Ω_0 and M_0 (independent of n)

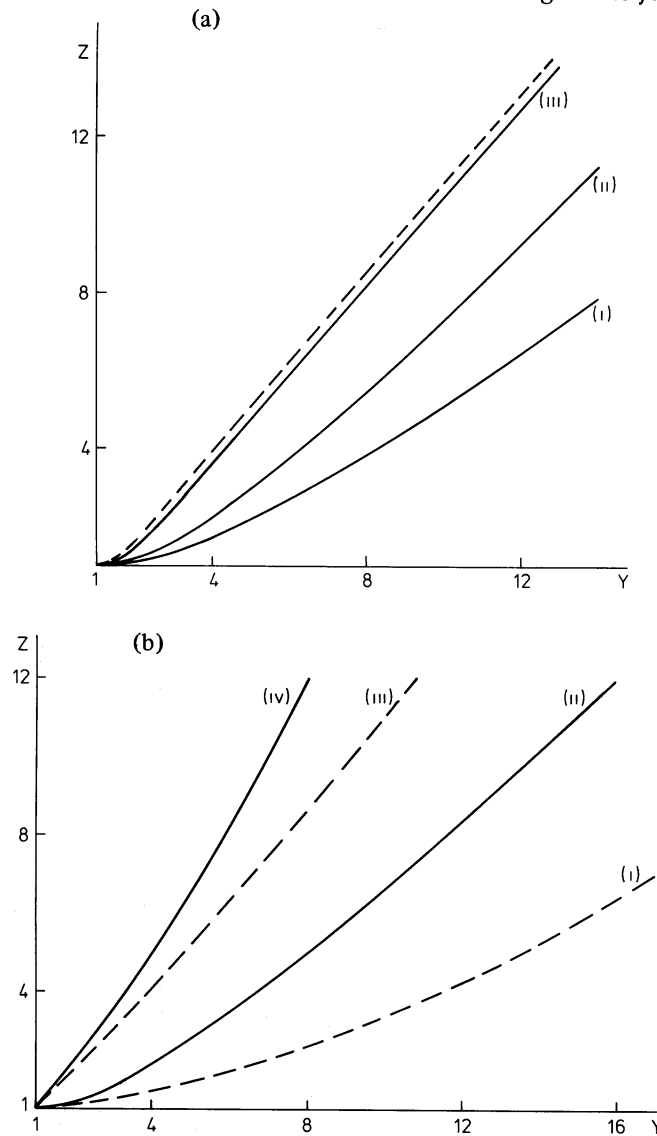$$\frac{\cos \Omega_F}{\cos \Omega_0} = (1 - \xi)^{1/2}, \tag{32}$$

Figure 3. (a) Jet paths for the initial conditions $\Omega_0 = 0$ and $\xi = {}^4/_7$ (corresponding to $M_0^2 = 1.5$ in the relativistic case). The curves are for power law atmospheres $p \propto z^n$ where (i) $n = -\frac{1}{2}$, (ii) $n = -1$, (iii) $n = -4$, and the dashed curve is the exponential atmospheres (equation 3). (b) Jet paths for the power law atmospheres with $\mu = -\frac{2}{3}$, with the initial conditions , (i) $\Omega_0 = 0°$, $\xi = \frac{1}{5}$; (ii) $\Omega_0 = 0°$, $\xi = \frac{1}{2}$; (iii) $\Omega_0 = 45°, \xi = \frac{1}{5}$, (iv) $\Omega_0 = 45°$, $\xi = \frac{1}{2}$.

as shown in Fig. 4. Large bendings ($\geqslant 40°$) will only occur in a jet satisfying both:

(i) an initially low Mach number flow ($M_0 \lesssim 2$); and

(ii) initially directed close to the major axis of the flattened confining gas cloud ($\Omega_0 \leqslant 10°$).

5.3 JET AREA AND CONFINEMENT

From the zero-order solution, the cross-sectional area, $A(z)$, is obtained. Equations (7) and (10) yield

$$\frac{A}{A_0} = z^{-n/\gamma} \left(\frac{1-\xi}{1-\xi z^\mu}\right)^{1/2}. \tag{33}$$
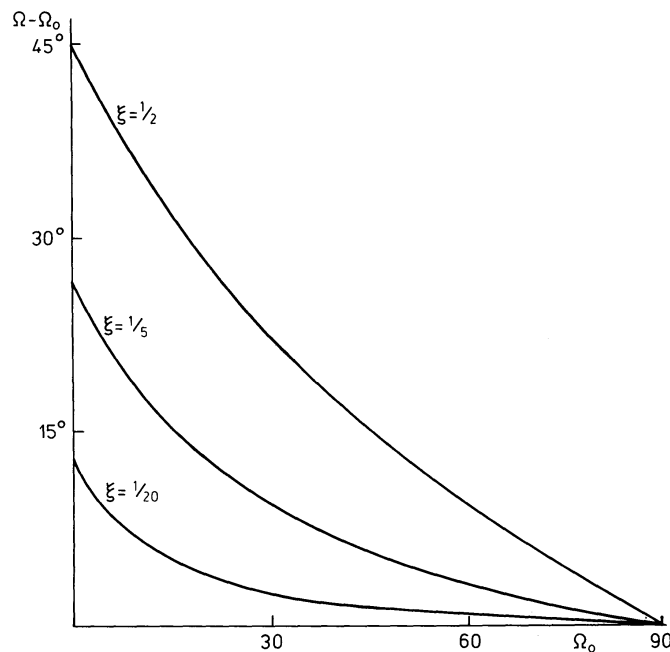
Figure 4. Total bending of jets as a function of the initial angle between the jet and the major axis of the gaseous disc.

Using equation (17), this can be expressed as $A\rho \cos \Omega = A_0\rho_0 \cos \Omega_0$, simply implying that the component of velocity perpendicular to the external pressure gradient remains constant.

The pressure balance requirement will break down when the transverse velocity of a fluid element in the jet approaches the internal sound-speed. Then, the flow pressure cannot fully respond to the external pressure changes. A 'free expansion' will result when the pressure difference between the jet and the external medium becomes large. The confinement condition is $\epsilon(dS/ds) \ll c_s/\Gamma v$. On the assumption that the jet keeps an approximately circular cross-section, this can be written as $\epsilon \, d(A/A_0)^{1/2}/ds \ll 1/M$. The true shape of the jet will be calculated in Paper II (Smith & Norman 1981). The above assumption implies that we are calculating a necessary condition for confinement, since the minimum expansion rate is being employed.

Using the above formulae, this condition can be written as

$$z^{n+2} \frac{2(\gamma-1)\gamma^2}{n^2} \geqslant \epsilon^2 \left(\frac{1-\xi}{\xi^2}\right)^{1/2} \left[1 - \cos^2 \Omega_0 \left(\frac{1-\xi}{1-\xi z^\mu}\right)\right] \left[1 - \frac{\xi z^\mu(1+\gamma)}{2}\right]^2 [1-\xi z^\mu]^{-3/2}. \quad (34)$$

By taking $n \sim -1.5$, $\gamma \sim 1.5$, and presuming that $\xi z^\mu \ll 1$, this becomes

$$z^{n+2} \geqslant \epsilon^2 \left(\frac{1-\xi}{\xi^2}\right)^{1/2} [1-(1-\xi) \cos^2 \Omega_0]. \quad (35)$$

If $n > -2$, i.e. slowly decreasing external pressures, then a jet that is confined at the initial stage will remain confined all along its length. If $n < -2$, the jet only remains confined for a finite length. As an example, we shall require the transverse fluid velocity to be less than $0.1 c_s$ and take an initially low Mach number flow with $\Omega_0 = 90°$ and $\epsilon = 0.03$. Then equation (35) yields $z < 10^{-1/(n+2)}$. If $n < -3$, then $z < 10$ and the jet remains confined for only a few scale-heights.

6 Observational implications

In general, jets exhibit curvature from a few degrees to ~ 60°. Three mechanisms for jet-bending will be considered:

(i) The central engine is time-variable, ejecting material in somewhat different directions.

(ii) The jet that we see is, in fact, an illumination of an inhomogeneous medium by a straight jet, but giving the illusion of a bent jet.

(iii) The interaction of the interstellar medium with the jet determines the path of a jet through the pressure balance requirement.

6.1 VARIABLE INJECTION

In the category of S-shaped sources, the trail of radio emission from the extended components does not align with the central core component. Such trails have a constant orientation on both sides of the core, but with a displacement of a few kiloparsecs, giving an overall 180° rotational symmetry about the core. Examples are 3C 47, 4C 13.21, 4C 37.43 (Miley & Hartsuijker 1978), 3C 382 and 3C 452 (Riley & Branson 1973). An explanation in terms of a gradual change in the initial jet direction (Miley 1976) cannot be ruled out, although in general this is expected to lead to much greater misalignments, such as that observed in NGC 326 (Ekers *et al.* 1978). There is definitely at least one class of jets which does not fall into this category because their curvature occurs predominantly in the inner regions.

6.2 VARIABLE ILLUMINATION

The interstellar medium in the central parts of the surrounding galaxy is likely to be very inhomogeneous. It has been suggested that interaction of the jet with such dense inhomogeneities may cause it to glow at random points, giving the illusion of jet-bending (Miley 1980).

Bending is an important phenomenon in quasars since VLBI observations have found curvature to be a common feature in radio components coincident with quasi-stellar sources (Readhead, Cohen & Blandford 1978). Note that the position angles of the elongated radio structures change systematically with distance from the nucleus (on the order of parsecs), through angles in the range 20–40°. In, for example, 3C 273 and 345, the curvature decreases with increasing distance; and the core orientations finally straighten in the direction of extended features. Such smooth behaviour is inconsistent with the hypothesis of illusory bending due to random cloud interaction with a straight jet.

6.3 PRESSURE GRADIENTS

We have argued that large bendings in jets produced by external pressure gradients should not be common. However, in a few quasars with superluminal expansions such large angles of bending are, in fact, observed. This conflict may be resolved if the jet is relativistic and the angle between the jet and the observer's line-of-sight is small. Jets bent through a few degrees will then appear to be strongly curved for most lines-of-sight almost parallel to the jet. Consequently, the bent-jet model implies that relativistic beaming towards the observer should be a common property of superluminally expanding sources with large bending angles. It has been proposed that the apparent superluminal separation speeds of radio components, and the ratio of radio-loud and radio-quiet quasars, can also be explained on this basis (Scheuer & Readhead 1979).

The theoretical jet-paths shown in Fig. 3(a) and (b) are consistent with the structure of S-shaped sources. Predicted misalignments between the initial and final paths of a jet are of the order of a few scale-heights; and rapid decrease in jet curvature thereafter can produce extended radio structures with a constant orientation.

Although jets can be bent up to $\sim 50°$, as has been observed for 3C 66B (Northover 1973), very particular initial conditions are required: a steady, low Mach number flow must be initially directed into the major plane of a highly flattened gas distribution. Since little bending is expected once the confining pressure has decreased by an order of magnitude from its initial value, substantial jet-bendings are restricted to the vicinity of the jet's source. High resolution studies of compact central components associated with extended sources will reveal further examples of jets that are being bent by as much as $50°$, if flattened confining gas distributions are prevelant.

Assuming an isotropic distribution of initial directions, from Fig. 4 it can be deduced that the 'average' jet-bending is very small — a few degrees only. The figure also predicts that there will be a scarcity of jets subtending small angles to the major axes of the confining clouds. This is consistent with studies of powerful radio sources associated with elliptical galaxies, carried out to determine whether a correlation exists between the orientation of the major axis of the radio structure and the major axis of the optical galaxy (angle Ω'). Guthrie's sample of 23 sources has orientations over all possible angles, but with a mean value of $\Omega' = 59°$, and only three sources with $\Omega' < 30°$ (Guthrie 1979). This deficiency is consistent with the bent-jet model on the assumption that there is a flattened confining gas cloud associated with the flattened optical image of the galaxy. A recent study of 78 sources by Palimaka *et al.* (1979) has revealed a similar preference for radio source alignment with the optical minor axis of the cores (the inner 10–20 kpc). The mean value of Ω' in this sample is $55°$. In addition, there is a marked trend for greater alignment as larger sources are taken: the mean values of Ω' for radio sources smaller and larger than 250 kpc are $49°$ and $68°$, respectively. (This fact and poor data explain the lack of definite correlation found by previous authors who considered few sources with linear sizes larger than 250 kpc).

It therefore seems that, besides the possibility of a jet-bending effect caused by pressure gradients external to the jet, other factors must be involved. Possible explanations for the trend are as follows:

(a) The alignment of axes ($\Omega' = 90°$) favours the development of large sources through greater jet stability or less dissipation of power on the walls of the jet.

(b) The jet orientation changes such that closer alignment is obtained as a source gets older (i.e. becomes larger).

(c) The precession of a jet around the core's minor axis spreads the ejected energy over a large solid angle, hindering the formation of distant radio lobes.

6.4 SPECIFIC RADIO SOURCES

We shall now consider more recent observations of jets and interpret their structure in terms of our model.

6.4.1 NGC 6251

From Cohen & Readhead (1979), we determine the initial (at 1 pc) jet direction to be given by $\Omega_0 = 78°$ and the final direction (at $\gtrsim 3$ kpc) by $\Omega_F = 83°$. Thus, the initial Mach number is $M_0 = 1.05/(\gamma - 1)$. For a relativistic jet, $\gamma = 2$ and $M_0 \sim 1$. Jet-bending occurs in NGC 6251 between 1 pc and 3 kpc. Using a pressure distribution as calculated by Readhead *et al.*

1978), with $n = -1.7$, we find the increase in Mach number with distance along the jet, s, is given by $M \sim \sqrt{3} \, s^{0.425}$. For $M \sim 1$ at 1 pc, we find $M \sim 50$ at 3 kpc, which is consistent with the estimate of $M \gtrsim 40$ given by Readhead *et al.* (1978).

The jet must have a low Mach number in the region where it is being bent. Thus, it probably has a rather large opening angle at ~ 1 pc and is only just proceeding to be focused through the nozzle point at this distance. However, the jet must be confined to be bent in our model, implying large pressures in the central region (Readhead *et al.* 1978). X-ray observation may give further indication of the pressure in the jet surroundings in the inner 1 pc of the galaxy (Blandford & Rees 1978).

6.4.2 3C 449

From the estimate of the Mach number ~ 8 at $\gtrsim 3$ kpc (Perley *et al.* 1979), we do not expect to see any bending of the jet.

6.4.3 3C 66B

The observed bending is $40°$. The jet must, therefore, be injected at a very large angle to the minor axis of the confining gas cloud. The initial direction of the jet is roughly parallel to the minor axis of the optical galaxy (Butcher, Van Breugel & Miley 1980) at ~ 2 kpc. Note that there is evidence that only one jet is bent on this scale; and therefore we expect the environment of the nucleus to be rather asymmetric.

6.4.4 NGC 1265

Our model has application to head—tail sources provided significant amounts of interstellar material are retained within the inner ~ 10 kpc of the galaxy. The ram pressure force on the interstellar medium will give rise to a pressure gradient across this region that deflects the jet (Jones & Owen 1979). From equation (39) it is obvious that the conditions for large degrees of bending are still applicable. Consequently, for the jets of NGC 1265, we require an initial Mach number $M_0 \sim 1$. The ejection angle (measured from the direction of ∇P) must be $\Omega_0 \lesssim 80°$, as observed. The slow widening and continued curvature of the jet can also be simulated.

6.4.5 3C 236

Using $\Omega_0 = 66°$, $\Omega_F = 72°$, we find $M_0 \sim 2$ at ~ 2 kpc. Note that there is evidence that only one jet is bent on this scale (Schillizi *et al.* 1979); and therefore we expect the gas distribution in the inner parts of the galaxy to be rather asymmetric.

In summary, it seems that the detailed calculation of jet trajectories in relation to observed properties of bent jets can provide quite significant constraints, both on the nature of jets themselves and on the gas distribution of the inner regions of active galaxies.

Acknowledgments

References

Abramowitz, M. & Stegun, I. A., 1965. *Handbook of Mathematical Functions,* Dover, New York.
Begelman, M. C., Rees, M. J. & Blandford, R. D., 1979. *Nature,* 279, 770.

Blandford, R. D. & Rees, M. J., 1974. *Mon. Not. R. astr. Soc.,* **169**, 395.
Blandford, R. D. & Rees, M. J., 1978. *Phys. Scripta,* **17**, 265.
Bridle, A. H., Davis, M. M., Fomalont, E. B., Willis, A. G. & Strom, R. G., 1979. *Astrophys. J.,* **228**, L9.
Butcher, H. R., Van Breugel, W. & Miley, G. K., 1980. *Astrophys. J.,* **235**, 749.
Cohen, M. H. & Readhead, A. C. S., 1979. *Astrophys. J.,* **233**, L101.
Ekers, R. D., Fanti, R., Lari, C. & Parma, P., 1978. *Nature,* **276**, 588.
Geer, J., 1977a. *Phys. Fluids,* **20**, 1614.
Geer, J., 1977b. *Phys. Fluids,* **20**, 1622.
Guthrie, B. N. G., 1979. *Mon. Not. R. astr. Soc.,* **187**, 581.
Jones, T. W. & Owen, F. N., 1979. *Astrophys. J.,* **234**, 818.
Keller, J. B. & Geer, J., 1973. *J. Fluid Mech.,* **59**, 417.
Keller, J. B. & Weitz, M. L., 1952. Inst. Math. Mech., New York University; Rep. IMM-NYU, p. 186.
Keller, J. B. & Weitz, M. L., 1957. 9th Int. Cong. Appl. Mech. (Brussels) pp. 316–323.
Landau, L. D. & Lifshitz, E. M., 1959. *Fluid Mechanics,* Pergamon Press.
Miley, G. K., 1976. *The Physics of Non-Thermal Radio Sources,* p. 1, ed. Setti, G., D. Reidel, Dordrecht.
Miley, G. K., 1980. *A. Rev. Astr. Astrophys.,* **18**, 165.
Miley, G. K. & Hartsuijker, A. P., 1978. *Astr. Astrophys. Suppl.,* **34**, 129.
Northover, K. J. E., 1973. *Mon. Not. R. astr. Soc.,* **165**, 369.
Palimaka, J. J., Bridle, A. H., Fomalont, E. B. & Brandie, G., 1979. *Astrophys. J.,* **231**, L7.
Perley, R. A., Willis, A. G. & Scott, J. S., 1979. *Nature,* **281**, 437.
Readhead, A. C. S., Cohen, M. H. & Blandford, R. D., 1978. *Nature,* **272**, 131.
Readhead, A. C. S., Cohen, M. H., Pearson, T. J. & Wilkinson, P. N., 1978. *Nature,* **276**, 768.
Riley, J. M., Branson, N. J., 1973. *Mon. Not. R. astr. Soc.,* **164**, 271.
Scheuer, P. A. G., 1974. *Mon. Not. R. astr. Soc.,* **166**, 513.
Scheuer, P. A. G. & Readhead, A. C. S., 1979. *Nature,* **277**, 182.
Schilizzi, R. T., Miley, G. K., van Ardenne, A., Baud, B., Baath, L., Ronnang, B. O. & Pauliny-Toth, I. I. K., 1979. *Astr. Astrophys.,* **77**, 1.
Smith, M. D., 1979. *D. Phil. Thesis,* Oxford University.
Smith, M. D. & Norman, C. A., 1981. *Mon. Not. R. astr. Soc.,* **194**, 785 (Paper II).
Tuck, E. O., 1976. *J. Fluid Mech.,* **76**, 625.
Van Breugel, W. & Miley, G. K., 1977. *Nature,* **265**, 315.

Extragalactic jets — II. Shape and stability

M. D. Smith *Department of Theoretical Physics, 1 Keble Road, Oxford OX1 3NP and Department of Physics, University of Illinois at Urbana-Champaign, Urbana, Illinois 61801, USA*

C. A. Norman *Huygens Laboratorium, University of Leiden, Wassenaarseweg 78, 2300 RA Leiden, The Netherlands*

Summary. A general formulation is given for determining the internal structure and stability of extragalactic jets confined by external pressure. Solutions are found for the jet cross-sectional shape and internal pressure distribution for high Mach number flows. With rapidly decreasing external pressures, a circular jet is found to be stable. A circular jet is found to become *unstable* and its cross-section to flatten with increasing jet-path length when the rate of decrease of external pressure is sufficiently slow. This global instability will lead to jet splitting and breakup.

1 Introduction

Detailed, high resolution maps of jets now allow us to infer not only jet trajectories, but also some aspects of internal jet structure and stability. We have therefore, undertaken a detailed extension of the trajectory calculations given in Paper I in order to model internal flow properties of jets. Once again, comparison of our model with the recent observations should provide further understanding of both jets and their environments.

First, we determine the cross-sectional shape to zeroth order in the slenderness parameter ϵ and the velocity potential and pressure up to order ϵ^2 for large distances from the jet's origin (Sections 2 and 3). Secondly, the equations for higher order terms are found; and, by generalizing the work of Geer (1977), we discuss the global instability of the jet cross-section to deformation (Section 4). Using these results, we then discuss the interpretation of observed properties of jets (Section 5).

The mathematical details are rather complex; and can be found in Smith (1979).

2 Cross-sectional shape of jets

2.1 DETAILED ANALYSIS

In Paper I, differential equations were obtained and solved for ϕ^0 and ϕ^1. In so doing, the jet curvature and cross-sectional area to zeroth order was obtained. Now higher-order coefficients are considered and solutions for ϕ^2 and S^0 are found.

The solution for $K \equiv 0$ with S^0 independent of θ (a straight circular jet) is

$$\frac{\partial \phi^2}{\partial r} = \frac{gr}{2},$$

$$\frac{\partial \phi^2}{\partial s} = \frac{\dot{g}}{4} \left\{ r^2 - (S^0)^2 \right\} - \frac{g^2}{8\dot{\phi}^0} (S^0)^2, \tag{1}$$

and

$$(S^0)^2 = c_0^2 (\dot{\phi}^0)^{-1} \{1 - (\dot{\phi}^0)^2\}^{1/(1-\gamma)},$$

where c_0 is a normalization constant so that $(S^0)^2 = A/A_0$,

$$g = \frac{2}{\gamma - 1} (\dot{\phi}^0)^2 \ddot{\phi}^0 [1 - (\dot{\phi}^0)^2]^{-1} - \ddot{\phi}^0 \tag{2}$$

and the dot represents differentiation with respect to s.

For $K \not\equiv 0$, we look for separable solutions. The equations are greatly simplified for high Mach number flows and the cross-section is an ellipse with semi-axes a and b given by

$$a = \left[\frac{-\dot{\beta}}{\dot{g}/4 + \dot{\alpha} + \frac{1}{2}(g/2 + 2\alpha)^2} \right]^{1/2},$$

$$b = \left[\frac{-\dot{\beta}}{\dot{g}/4 - \dot{\alpha} + \frac{1}{2}(g/2 - 2\dot{\alpha})^2} \right]^{1/2}. \tag{3}$$

The semi-axis in the y–z plane ($\theta = 0°$) is a, and the semi-axis in the x-direction ($\theta = 90°$) is b.

The separable solution leads to a particular solution for ϕ^2 and S^0 that results in a jet with an elliptical cross-section.

The general solution for high Mach number flows yields

$$\ddot{\eta} = (\dot{g} + \frac{1}{2}g^2) \frac{1 - \eta^2}{1 + \eta^2} \eta - \dot{\eta}g + \frac{1}{2} \frac{\dot{\eta}^2}{\eta} \frac{3 + \eta^2}{1 + \eta^2}, \tag{4}$$

where $\eta = a/b$ is the aspect ratio. By the change of variables $s \equiv \exp(t)$, this can be written as

$$\frac{\partial \eta'}{\partial \eta} = 1 + \frac{n}{\gamma} + \frac{n}{2\gamma} \left(\frac{n}{\gamma} + 2 \right) \frac{\eta}{\eta'} \frac{1 - \eta^2}{1 + \eta^2} + \frac{1}{2} \frac{\eta'}{\eta} \frac{3 + \eta^2}{1 + \eta^2}. \tag{5}$$

Here, the dashes denote differentiation with respect to t. If $\eta(t)$ is a solution to equation (5), then so is $1/\eta(t)$. The problem is independent of whether we take the aspect ratio as a/b or b/a. The aspect ratio can be studied by consideration of trajectories in the η, η' phase plane.

A further solution is a jet with a circular cross-section given by $\alpha = 0$.

2.2 ILLUSTRATIONS OF JET SHAPES

We graph the solution of equation (5) in Figs 1 to 4. The jet shape in the limit as $s \to \infty$ is strongly dependent on n/γ, as we discuss below. In all graphs, the arrows denote the direction of increasing jet arc length. An important point to note is that if η' is replaced by $-\eta'$ and $(1 - n/\gamma)$ by $(1 + n/\gamma)$, then the value of $\partial \eta'/\partial \eta$ keeps the same magnitude but changes its sign. Hence the diagram for $(1 - n/\gamma)$ is simply the mirror-image of the diagram

for $(1 + n/\gamma)$, with the reflection about the $\eta' = 0$ axis and the directions of increasing s reversed.

Fig. 1, specifically for $n/\gamma = -3$, is representative of the change in jet shape with arc length for $n/\gamma < -2$. Given any initial conditions η and η' where the high Mach number approximation is valid, the final shape of the jet can be immediately determined from the figure. In this case, all the trajectories spiral in towards the stable point $\eta = 1, \eta' = 0$, that is, the circular jet. In the limit as $s \to \infty$ and $\eta \to 1$, the ellipticity oscillates between negative and positive values with a rapidly decreasing amplitude of oscillation. The decrease of the amplitude of the spiral is a factor $\exp(2\pi) \sim 500$ per revolution around $\eta = 1$ as $\eta \to 1$ and with $-n/\gamma \gg 2$, and a factor $\exp(2\pi\sqrt{2}) \sim 7000$ per revolution for Fig. 1. Therefore, very few oscillations can be seen in the figure.

Fig. 2 is a special case $n/\gamma = -2$, in which the ellipticity remains bounded and $\eta' \to 0$ in the limit as $s \to \infty$. Consequently, if $n/\gamma \leq -2$ and initial conditions of the form $\eta \sim 1, \eta' \ll 1$ are given, then the aspect ratio does not vary significantly from unity. Furthermore, the ellipticity remains bounded for all initial conditions.

Fig. 3, specifically for $n/\gamma = -\frac{3}{2}$, is representative of the jet shape for $-2 < n/\gamma < -1$. An initially circular jet with $\eta' = 0$ is now highly unstable. Initial conditions in the neighbourhood of this point result in a jet in which $\eta \to 0$ or $\eta \to \infty$. Hence, in all cases, $\eta \to 0$ or $\eta \to \infty$, in the limit as $s \to \infty$.

Fig. 4 is the special case $n/\gamma = -1$ in which there is reflection symmetry about the $\eta' = 0$ axis. The form of the trajectories in the range $-1 < n/\gamma < 0$ can be obtained by reflecting Fig. 3 about the $\eta' = 0$ axis. Therefore, in the range $-2 < n/\gamma < 0, \eta \to 0$ or ∞ in the limit as $s \to \infty$.

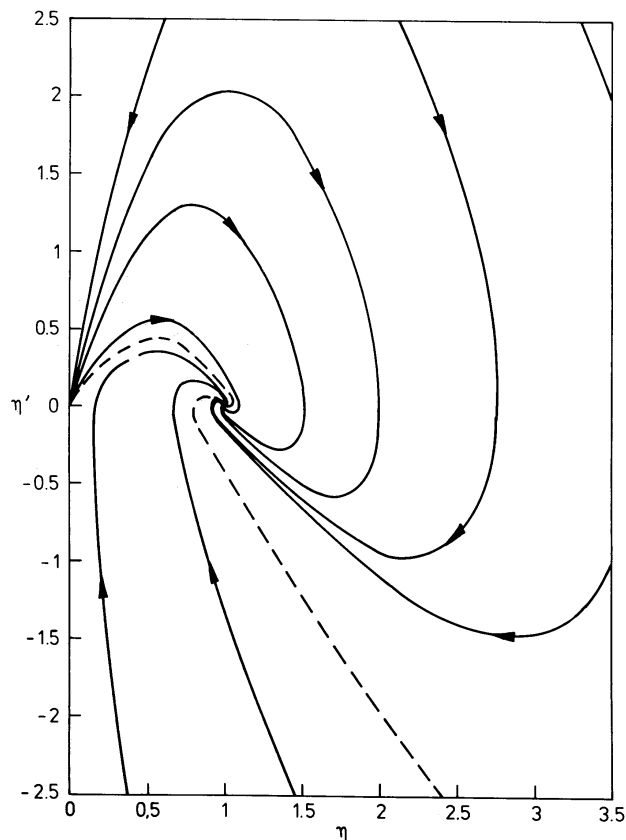**Figure 1.** Phase plane trajectories for $n/\gamma = -3$ (see text). The arrows denote the direction of increasing jet arc length.
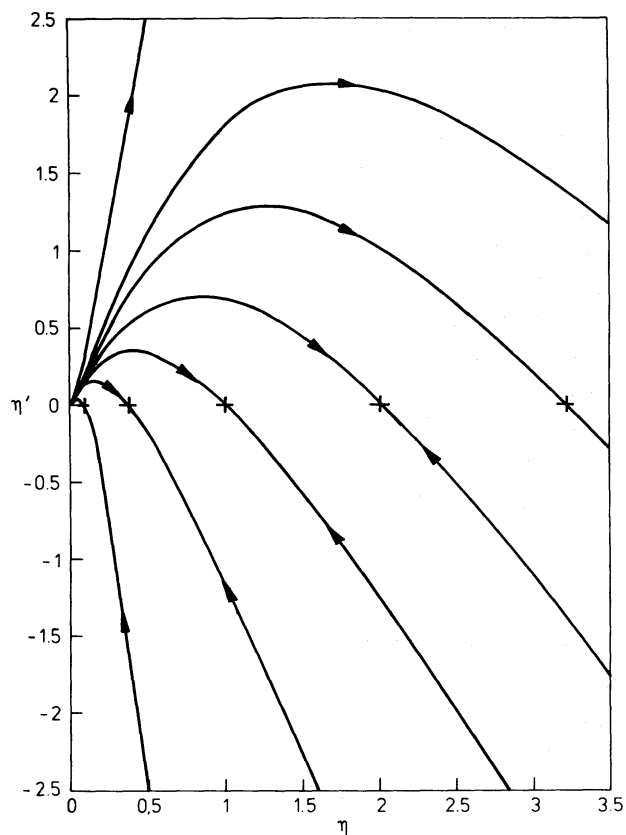
788   *M. D. Smith and C. A. Norman*

Figure 2. Phase plane trajectories for $n/\gamma = -2$ (see text). The crosses denote the stable point on each trajectory.
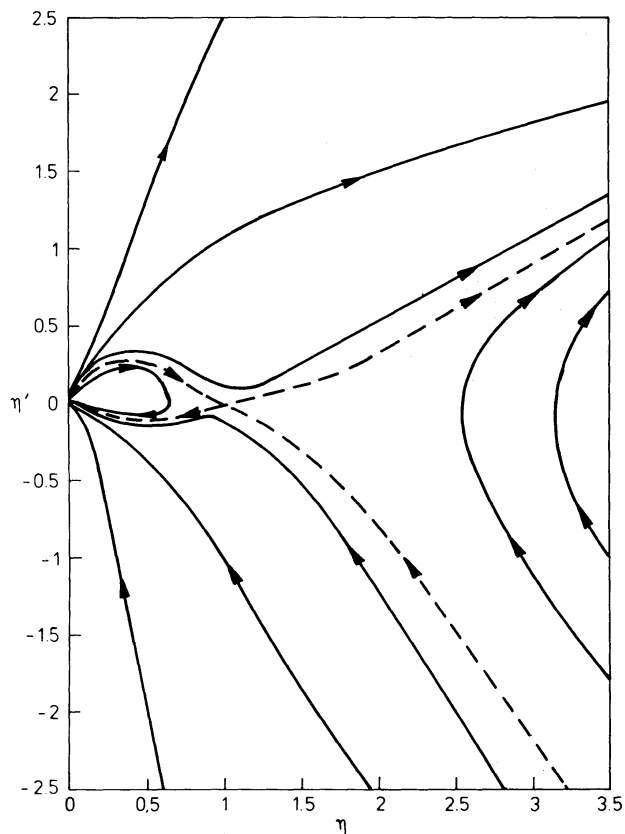

Figure 3. Phase plane trajectories for $n/\gamma = -\frac{3}{2}$ (see text).
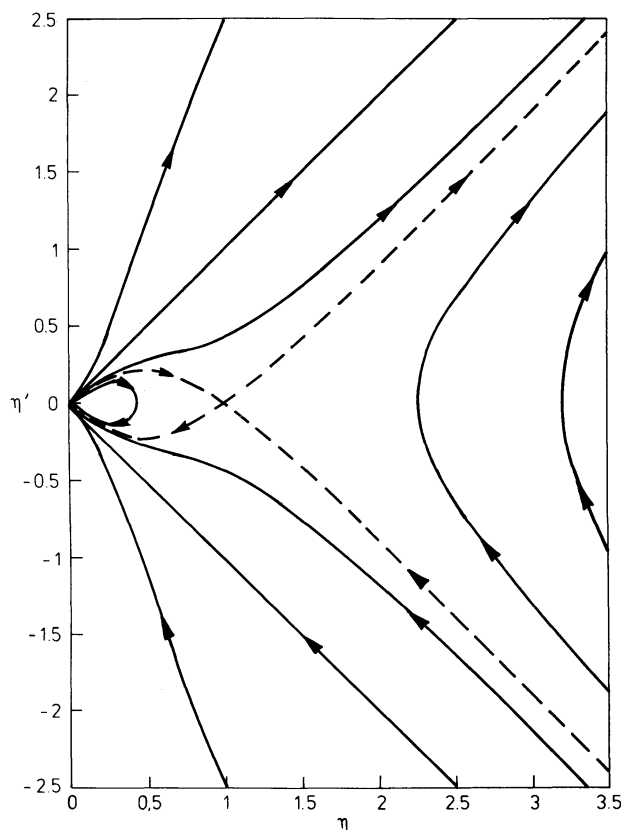
Figure 4. Phase plane trajectories for $n/\gamma = -1$ (see text).

In the determination of S^0 it has been assumed that the slenderness approximations are still valid at large distance from the origin of the jet, despite the possible degeneration of the jet into a sheet. In equation (20) of Paper I, the term $(\dot{\phi}^0)^2 \ddot{\phi}^0$, which is of the order of ϵ^4, was ignored when deriving ϕ^0 and ϕ^1. Since, in the limit as $s \to \infty$, $z \propto s$, it follows that $(\dot{\phi}^0)^2 \ddot{\phi}^0 = 0(s^{\mu-1})$; and so, with $\mu < 0$, the approximation made in equation (20) is valid. Similarly, in Paper I, the terms of order ϵ^2 and ϵ^4 in equations (21) and (22), respectively, were ignored in deriving ϕ^0 and ϕ^1. We now calculate that these are $\dot{s}^0 \dot{\phi}^0 = O(1)$ and $(\dot{\phi}^0)^2 - 1 + \xi z^\mu = O(1)$, in the limit as $s \to \infty$; and hence, our results are consistent with the original approximations.

We have determined the boundary surface of a jet with an elliptical cross-sectional shape in the case of a high Mach number flow. Examples of boundary surfaces are shown in Fig. 5, where an initial jet angle of injection of $\Omega = 90°$ has been chosen. The width is displayed in the y-direction, and the breadth in the x-direction.

If $0 > n/\gamma > -2$, the jet degenerates into a sheet of fluid whose width increases in proportion to the arc length. Consequently, the jet will appear to be conical (Fig. 5a,b,c). Furthermore, if $n/\gamma > -1$, the thickness of the sheet decreases to zero in the limit as $s \to \infty$ (Fig. 5a). If $n/\gamma < -1$, then both the width and thickness approaches infinity in the limit as $s \to \infty$ (Fig. 5c). If $n/\gamma < -2$, the jet cross-section will approach a stable circular shape via oscillations (in the ellipticity) of decreasing amplitude in the limit as $s \to \infty$. The axes become of the order of $s^{-n/2\gamma}$, and so the boundary streamlines diverge away from the locus of centroids (Fig. 5d).

The confinement condition derived in Paper I will not hold in the case of $n/\gamma > -2$, since it has been shown that the circular cross-section assumption is invalid. Therefore, we now
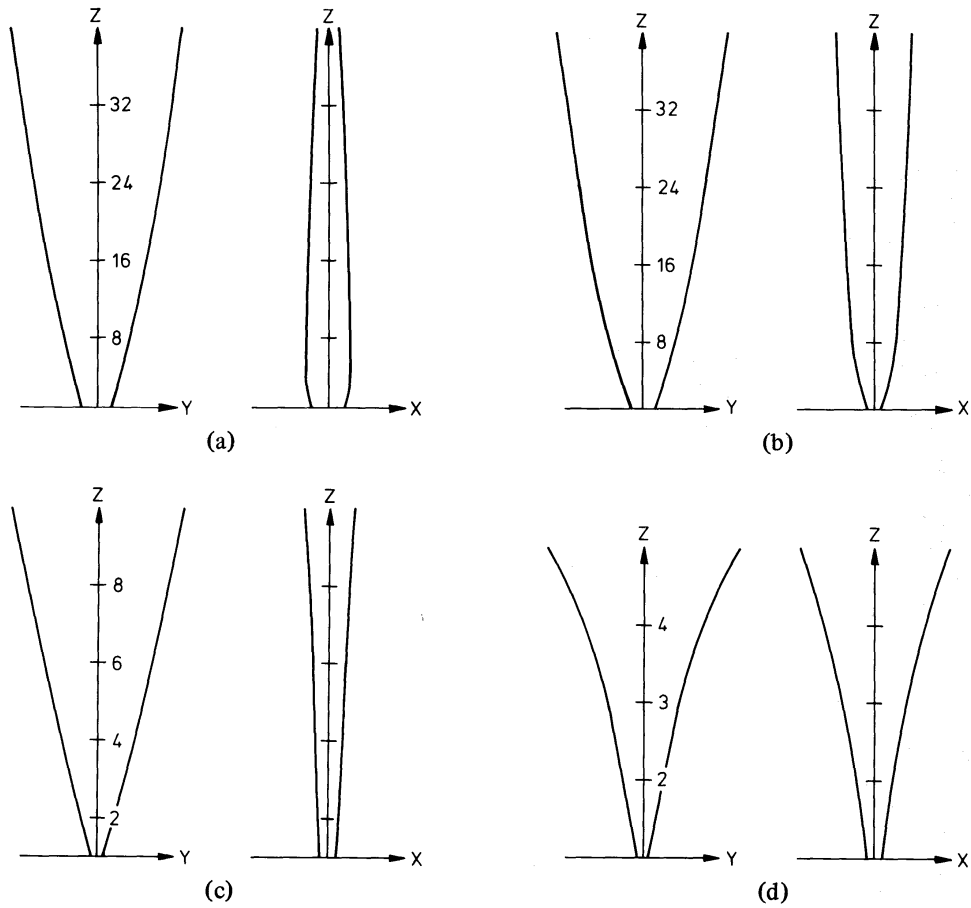
Figure 5. (a) Boundary surface of a jet with $\xi = 0$, $n/\gamma = -\frac{1}{2}$ and initial conditions $\eta = 1$, $\dot{\eta} = 0.1$. (b) Boundary surfaces with $\xi = 0$, $n/\gamma = -1$ and initial conditions $\eta = 1.75$, $\dot{\eta} = -0.5$. (c) Boundary surfaces with $\xi = 0$, $n/\gamma = -\frac{3}{2}$ and initial conditions $\eta = 0.8$, $\dot{\eta} = 0.8$. (d) Boundary surfaces with $\xi = 0$, $n/\gamma = -3$ and initial conditions $\eta = 0.8$, $\dot{\eta} = 0.8$.

write the confinement condition as $\epsilon(da/ds) \ll 1/M$ and $\epsilon(db/ds) \ll 1/M$. Applying the asymptotic formulae for the jet shape as given here by equation (16) and by equation (50) of Paper I, this confinement condition becomes

$$\epsilon^2 \ll \xi z^{\mu}. \tag{6}$$

Stipulating the transverse velocity to be less than one-tenth of the sound-speed of the jet, the confinement condition can be written as

$$z^{-n} < 10^{\gamma/(\gamma-1)} \left(\frac{\xi}{0.1}\right)^{-\gamma/(\gamma-1)} \left(\frac{\epsilon}{0.01}\right)^{2\gamma/(\gamma-1)}. \tag{7}$$

Thus, confinement can be maintained up to $z \gtrsim 10$ for all $n > -2$ and $\gamma \lesssim 2$, for $\epsilon \sim 0.01$ and $\xi^2 \sim 0.01$.

The introduction of expansions ϕ^j and S^j in powers of ξ also gives a relationship between ξ and ϵ. In obtaining the zero- and first-order results, $\dot{\phi}^0 = 1$ and $\dot{\phi}^1 = 0$, the terms ignored were of the order ϵ^2 and ξz^{μ}. Since $\dot{\phi}^2$ is of the order ϵ^2, for correct ordering we require $\epsilon^2 \geqslant \xi z^{\mu}$, in contradiction to the confinement condition (19). Obviously, in ϕ^0 the expansion in ξ is not valid. Nevertheless, it is still possible to expand ϕ^2 and S^0 in powers of ξ, i.e. $\dot{\phi}^0 = 1 - \xi z^{\mu}$, $\phi^2 = \phi_0^2 + \phi_1^2 \xi + \phi_2^2 \xi^2 + \ldots$; and it follows that ϕ_0^2 has been correctly calculated here.

We have demonstrated that the width of the jet expands uniformly for $n/\gamma > -2$, large s and under external pressure confinement. Observations have shown that resolved jets often do have such a constant opening angle, with estimates of $n > -2$ (and hence, $n/\gamma > -2$ if $\gamma > 1$). Since an unconfined expansion can result in a conical jet, a free-jet model has been proposed (Readhead, Cohen & Blandford 1978; Perley, Willis & Scott 1979). We point out that, in the direction that gives greatest resolvability of the width, a confined beam will also be conical in shape.

3 Internal jet pressure distribution

The pressure distribution within the jet is found via the Bernouilli equation. For a circular jet, we obtain

$$\left(\frac{p}{p_0}\right)^{1-1/\gamma} = z^\mu + \frac{\epsilon^2}{4\xi}(g^2 + 2\dot{\phi}^0 \dot{g})[(S^0)^2 - r^2]. \tag{8}$$

The z^μ term signifies the pressure equilibrium with the surrounding medium at $r = S^0$. In the limit as $s \to \infty$, we find that $g^2 + 2\dot{\phi}^0 \dot{g} \to \frac{1}{2}n/\gamma (n/\gamma + 2)$. Thus, if $n/\gamma > -2$, the pressure decreases as r decreases, i.e. the radial pressure force is inhibiting the jet from expanding and the opening angle of the jet decreases with increasing arc length. If $n/\gamma < -2$, then the radial pressure force is acting outwards, and the bounding streamlines curve away from the centre of the jet.

Taking $\xi = 2(\gamma + 1)$, corresponding to $M_0 = 1$, and putting $z = 1$, then $\dot{\phi}^{0^2} = (\gamma - 1)/(\gamma + 1)$, $\ddot{\phi}^0 = -n/\gamma [(\gamma - 1)/(\gamma + 1)]^{1/2}$, giving $g = 0$ and $\dot{g}\dot{\phi}^0 = (n/\gamma)^2(\gamma - 1)$. When the flow is transonic, the radial pressure force is found to be always positive, tending to expand the jet. The outward-pressure force may inhibit the Kelvin–Helmholtz instability in the neighbourhood of the nozzle. The radial pressure gradient is reversed at large distances from the nozzle for the circular jet if $n/\gamma > -2$; and the entrainment of surrounding material could be significant.

The transverse expansion of a jet by pressure forces implies a lower velocity and a greater mass flux per unit area along the centroid of the jet than at the jet surface. This contrasts with models invoking higher central velocities resulting from frictional forces decelerating the fluid at the boundary surface.

In the more general non-axisymmetric case, the internal pressure distribution is given by:

$$\left(\frac{p}{p_0}\right)^{1-1/\gamma} = \left(\frac{p_1}{p_0}\right)^{1-1/\gamma} - \frac{\epsilon^2}{\xi} 2\dot{\phi}^0 c^2 \dot{\beta} \left[1 - \frac{r^2}{(S^0)^2}\right], \tag{9}$$

where p_1 is the pressure in the external medium. If $\dot{\beta} < 0$, the pressure within the jet is greater than the external pressure p_1; and conversely, if $\dot{\beta} > 0$, then $p < p_1$. The parameter $\dot{\beta}$ can be calculated for large s in the case $\xi = 0$. For $n/\gamma < -2$, the circular cross-sectional jet solution is approached in the limit as $s \to \infty$; and, $\dot{\beta} < 0$. If $-1 > n/\gamma > -2$, then $\dot{\beta}$ is positive; if $0 > n/\gamma > -1$, then $\dot{\beta}$ is negative (Smith 1979). The direction of the pressure gradient at the boundary surface may have considerable influence on the stability of the jet.

4 Jet stability

The internal structure of the jet has been determined by solving the non-linear boundary value problem for Poisson's equation. The application of initial conditions leads to a unique solution that was specified for jets with an elliptical or circular cross-sectional shape.

However, the solutions for ϕ^k and S^{k-2} with $k > 2$ are dependent on the particular solution found for ϕ^2 and S^0; but, even after the initial conditions are given, solutions for ϕ^k and S^{k-2} are not unique.

For the case of an incompressible fluid under gravity, Geer (1977) demonstrated that there exist non-trivial eigensolutions which have a physical interpretation in terms of the stability of the flow. For this reason, the problem will be limited to obtaining eigensolutions and determining the jet stability (Smith 1979).

For the circular jet in which the jet path is aligned with the external pressure gradient, we find that the cross-sectional shape is stable for $n/\gamma < -2$. As suggested in Figs 1–4, the circular jet is unstable in the rate $0 > n/\gamma > -2$. This can be interpreted physically by consideration of the centrifugal forces on the jet boundary. For $n/\gamma < -2$, the boundaries are convex (Fig. 5d) and the centrifugal forces are directed inwards, and act to stabilize the jet. For $0 > n/\gamma > -2$, the boundaries are concave, and a flattening of the beam will lead to greater outward centrifugal forces in the direction of flattening.

For an elliptical jet, the stable circular cross-section is approached as $s \to \infty$ for $n/\gamma < -2$. For $0 > n/\gamma > -2$, the jet is stable to disturbances that are *symmetric* about the plane into which the jet eventually flattens. However, the jet is spatially *unstable* to disturbances that are *asymmetric* about the plane into which the jet eventually flattens.

5 Observational implications and conclusions

The final jet cross-sectional shapes produced by this model can now be summarized.

(i) If $n/\gamma < -2$, a stable circular jet is attained, after possible oscillations in ellipticity about the circular state.

(ii) If $n/\gamma < -2$, a flattened jet results with an axial ratio proportional to $s^{n/\gamma + 2}$, where s is the distance along the jet. The two axes are proportional to s and $s^{-1-n/\gamma}$.

(iii) If $n/\gamma < -2$, the jets are unstable.

For example, the existence of the eigensolutions discussed above shows that flattening jets will tend to warp about their major axes, leading to a distortion and possibly a splitting of the jets as they continue to flatten. Although the final structure of an unstable jet is still somewhat uncertain owing to our ignorance of the non-linear regime of instability we can conclude in general that, if the confining external pressure distribution falls off sufficiently slowly ($n \lesssim 0$) along the jet, the jet will be deformed and eventually break up.

From statistical studies of radio sources, Pacholczyk (1977) and Valtonen (1979) estimate n to be in the range of $-2 > n > -3.5$, for either a free or a confined jet model. If the jet is confined by the pressure of material in the radio lobe, consisting of previously ejected fluid, then $n \sim 0$ (Scheuer 1974).

The jet length over which the confinement condition (equation 7) holds is proportional to $10^{1/n[\gamma/(\gamma-1)]}$; and the maximum growth-rate of an unstable mode is proportional to $s^{2+n/\gamma}$. Thus, if n is close to zero, the spatial instabilities discussed here should be significant enough to create observable jet distortion and fragmentation.

Finally, we emphasize that the flattening instability presented here for any confined jet with $n/\gamma > -2$, is quite different from other jet instabilities, such as the Kelvin–Helmholtz instability, (Turland & Scheuer 1976; Blandford & Pringle 1976; Hardee 1979), or the firehose instability, which are temporally growing modes. Here the flow remains time independent, but the amplitude of a disturbance grows with distance from the origin. All these instabilities evolve from centrifugal forces: the Kelvin–Helmholtz modes are local surface disturbances, the firehose mode arises from disturbances on scales larger than the jet

width, and these spatial instabilities arise from the intermediate scale of disturbance — the jet cross-section. However, the spatial instability will only result if there is some permanent slight distortion to the beam shape at some point along the beam path. While numerical techniques will be required for the more general investigation of jet shape and stability, particularly for low Mach number flows, the analytic bent-jet model given here seems to deal neatly with slender high Mach number jets.

Acknowledgments

References

Blandford, R. D. & Pringle, J. E., 1976. *Mon. Not. R. astr. Soc.,* **176**, 443.
Geer, J., 1977. *Phys. Fluids, 20,* 1622.
Hardee, P. E., 1979. *Astrophys. J.,* **234**, 47.
Pacholczyk, A. G., 1977. *Radio Galaxies,* Pergamon Press.
Perley, R. A., Willis, A. G. & Scott, J. S., 1979. *Nature,* **281**, 437.
Readhead, A. C. S., Cohen, M. H. & Blandford, R. D., 1978. *Nature,* **272**, 131.
Scheuer, P. A. G., 1974. *Mon. Not. R. astr. Soc.,* **166**, 513.
Smith, M. D., 1979. *D. Phil. Thesis,* Oxford University.
Smith, M. D. & Norman, C. A., 1981. *Mon. Not. R. astr. Soc.,* **194**, 771 (Paper I).
Turland, B. D. & Scheuer, P. A. G., 1976. *Mon. Not. R. astr. Soc.,* **176**, 421.
Valtonen, M. J., 1979. *Astrophys. J.,* **231**, 312.